

## Strong Coupling between Surface Plasmon Polaritons and Molecular Vibrations

H. Memmi, O. Benson, S. Sadofev, and S. Kalusniak

*Institut für Physik, Humboldt Universität zu Berlin, Newtonstrasse 15, 12489 Berlin, Germany*

(Received 14 March 2016; revised manuscript received 16 January 2017; published 23 March 2017)

We report on the strong coupling of surface plasmon polaritons and molecular vibrations in an organic-inorganic plasmonic hybrid structure consisting of a ketone-based polymer deposited on top of a silver layer. Attenuated-total-reflection spectra of the hybrid reveal an anticrossing in the dispersion relation in the vicinity of the carbonyl stretch vibration of the polymer with an energy splitting of the upper and lower polariton branch up to 15 meV. The splitting is found to depend on the molecular layer thickness and saturates for micrometer-thick films. This new hybrid state holds a strong potential for application in chemistry and optoelectronics.

DOI: [10.1103/PhysRevLett.118.126802](https://doi.org/10.1103/PhysRevLett.118.126802)

The hybridization of different quasiparticles is of both fundamental and practical interest. The resultant hybrid excitations exhibit new properties not available by the isolated constituents. We name here only microcavity polaritons built up by excitons and photons [1]. Coupling electromagnetic radiation and excitations in condensed matter in an appropriate setting has enabled the demonstration of phenomena like lasing without inversion [2], Bose-Einstein condensation [3], and superfluidity [4]. Another quasiparticle of considerable applied importance is the surface plasmon polariton (SPP) [5]. The coupling of surface plasmons with emitters has been extensively investigated, but only recently has the hybridization with excitons in organic and inorganic compounds received much attention [6]. In particular, organic  $J$  aggregates with an extraordinary large excitonic dipole moment have been employed [7–9], but hybridization with quantum well and quantum dot excitons have also been successful [10,11]. Spatial coherence properties [12,13] and in the time domain ultrafast Rabi oscillations [14], both fingerprints of the hybrid nature, have been demonstrated. Another molecular excitation located at much longer wavelengths are vibrational transitions. Plasmon-induced field enhancement is routinely exploited to intensify their signatures in surface-enhanced Raman spectroscopy allowing for direct infrared detection down to the single-molecule level [15,16]. The background physics has been widely studied with localized plasmons in metal nanostructures [17] but also on planar or islandlike metal surfaces [18–20]. Despite the experimental efforts, the strong coupling of SPPs and molecular vibrations has not yet been reported.

In this Letter, we demonstrate the strong coupling of SPPs and the stretch vibration of the carbonyl group of a ketone-based polymer. As this vibration involves predominantly only two atoms, our findings can be distinguished from previous work done on the strong coupling of SPPs and phonons [21].

The metal used in this study is silver, which is thermally evaporated on the base of a calcium fluoride hemicylindrical

prism resulting in layers with a controlled thickness of 25–35 nm and a root mean squared surface roughness below 3 nm. On the organic side, we employ the commercially available polymer poly(vinyl-methylketone) (PVMK). The molecular layer is spin-coated from a PVMK/chloroform solution on top of the silver layer to form the hybrid structure. The organic layer thickness is controlled within an accuracy of  $\pm 10\%$  as confirmed by atomic-force-microscopy measurements and optical transmission measurements on PVMK reference films deposited on silicon substrates. Evanescent waves are excited by attenuated-total reflection (ATR) in the Kretschmann-Raether configuration using the calcium fluoride prism as the coupling medium [Fig. 1(a)]. To obtain absolute values of the reflectivity, reference spectra of the sole hemicylindrical prism are measured. The angle of incidence  $\alpha$  is set with an accuracy of  $\pm 1^\circ$  in all experiments, and the angular spread of the excitation beam is  $\pm 1.75^\circ$ . All optical spectra are recorded with a resolution of  $4 \text{ cm}^{-1}$  by a Bruker IFS66v/s vacuum Fourier transform spectrometer.

To begin with, we discuss the optical properties of the organic material used in this study. The PVMK polymer is an acyclic ketone-based polymer with a single carbonyl group per repeating unit, as depicted in Fig. 1(b). A well-defined and strong signal related to the stretch vibration of the carbonyl group is found in the transmission spectrum of a 1360-nm-thick PVMK film spin-coated on top of a silicon substrate [Fig. 1(b)]. Reproducing the transmission spectrum by transfer matrix (TRMA) calculations and treating the vibrational transition as a Lorentzian resonance

$$\epsilon_m(\omega) = \epsilon_{bm} \left( 1 + \frac{A}{\omega_0^2 - \omega^2 - 2i\omega\gamma} \right) \quad (1)$$

allows for the extraction of the resonance frequency  $\omega_0 = 0.2119 \text{ eV}$ , the transition strength parameter  $A = 298 \text{ meV}^2$ , which is directly proportional to the density of carbonyl groups, and the dissipation rate

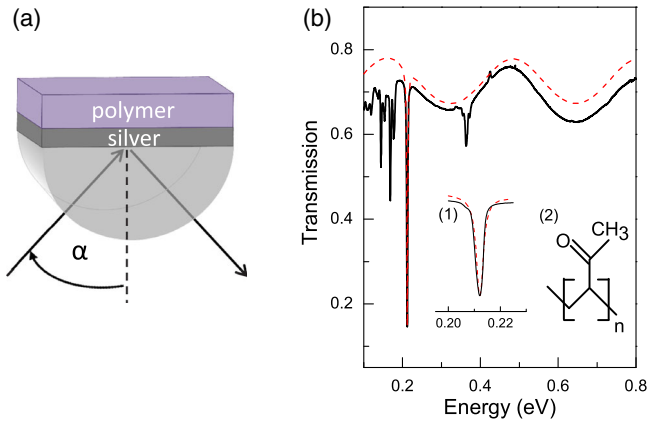


FIG. 1. (a) Schematics of the ATR measurements in the Kretschmann-Raether configuration using a calcium fluoride hemicylindrical prism as the coupling medium. The in-plane wave vector  $k = (\omega/c)\sqrt{\epsilon_{\text{CaF}_2}} \sin \alpha$  is experimentally defined by the angle of incidence  $\alpha$ . (b) Transmission spectrum of a 1360-nm-thick layer of PVMK on silicon in TM polarization ( $\alpha = 45^\circ$ ). Full black curves: Experiment. Dashed red curves: TRMA calculations. Inset 1: Enlargement of the transmission signal of the stretch vibration of the carbonyl group. Inset 2: Repeating unit of the PVMK polymer.

( $\gamma = 1$  meV) of the vibrational resonance. The midinfrared background permittivity  $\epsilon_{bm} = 2.50$  and PVMK layer thickness are deduced from the amplitude and position of the interferences fringes. For all other vibrational transitions in the investigated spectral range,  $A$  is more than a factor of 2 smaller, and for simplicity these transitions are omitted in the dielectric function. To ensure the validity of the dielectric function, we have varied the thickness of the PVMK film between 300 and 1600 nm and achieved similar good agreement between the experiment and theory.

Figure 2 depicts the ATR spectra of a PVMK/silver hybrid structure in the vicinity of the molecular resonance. While the ATR spectra show only a very weak molecular signal in transverse electric polarization (not shown), two pronounced minima appear in transverse magnetic (TM) polarization [Fig. 2(a)]. The upper branch (UB) shows up as a narrow minimum located slightly above the molecular resonance frequency. It shifts to higher energies and broadens significantly when increasing the angle of incidence. The lower branch (LB), on the other hand, approaches the molecular resonance from the low-energy side when  $\alpha$  is increased. If  $\alpha$  is very large, a weak signal with no detectable dispersion is also present at the molecular resonance frequency (middle branch). The experimental data are reproduced by TRMA calculations taking into account the calcium fluoride hemicylindrical prism as a semi-infinite medium [with  $\epsilon_{\text{CaF}_2}(\omega)$  taken from Ref. [22]], the silver layer, the polymer film, as well as air again as a semi-infinite medium. The dielectric function of the polymer [ $\epsilon_m(\omega)$ ] used in the TRMA calculations is

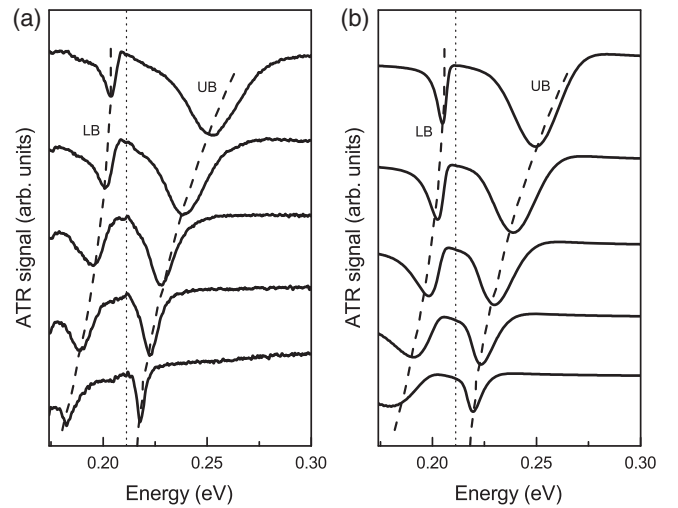


FIG. 2. TM-polarized ATR spectra of a PVMK/silver hybrid structure in the strong coupling regime. The silver and PVMK layer thickness is 29 and 965 nm, respectively. (a) Experimental spectra. (b) Corresponding TRMA calculations. The angle of incidence changes for all curves from  $\alpha = 60^\circ$  to  $68^\circ$  in steps of  $2^\circ$  (bottom to top). UB, upper branch; LB, lower branch. Dashed lines follow the ATR minima. The dotted line marks the molecular resonance frequency  $\omega_0$ . For parameters used in the TRMA computations, see the text.

obtained from the fitting procedure presented in Fig. 1(b). For silver, the best agreement between the experiment and theory is obtained using the dielectric function data of Ref. [23], which can be well approximated by Drude's dielectric function

$$\epsilon_p(\omega) = \epsilon_{bp} - \frac{\omega_p^2}{\omega(\omega + i\Gamma_p)} \quad (2)$$

in the relevant spectral range, with background contribution  $\epsilon_{bp} = 3.7$ ,  $\omega_p = 9.2$  eV the plasma frequency, and  $\Gamma_p = 26$  meV the electron scattering rate. While at fixed  $\alpha$  the position of the ATR minima in theory agrees well with the experimental data, the amplitude and width of the features cannot be reproduced. However, when accounting for the experimental angular spread of  $\pm 1.75^\circ$  in the TRMA calculations [24], good agreement between the experiment and theory is obtained [Fig. 2(b)]. The spectral width of both branches is thus governed by the angular spread of the excitation beam and not by the intrinsic decay rates.

Figure 3(a) depicts the observed ATR minima together with numerically calculated dispersion curves. In a first test, the experimental data are analyzed using the linear dispersion theory of a metal and dielectric half-space system [6]. Then, the complex energies of the upper (+) and lower (-) branch in resonance follow from

$$\omega_{\pm} = \omega_0 - \frac{i}{2}(\gamma + \gamma_{\text{spp}}) \pm \frac{1}{2}\sqrt{A - (\gamma - \gamma_{\text{spp}})^2} \quad (3)$$

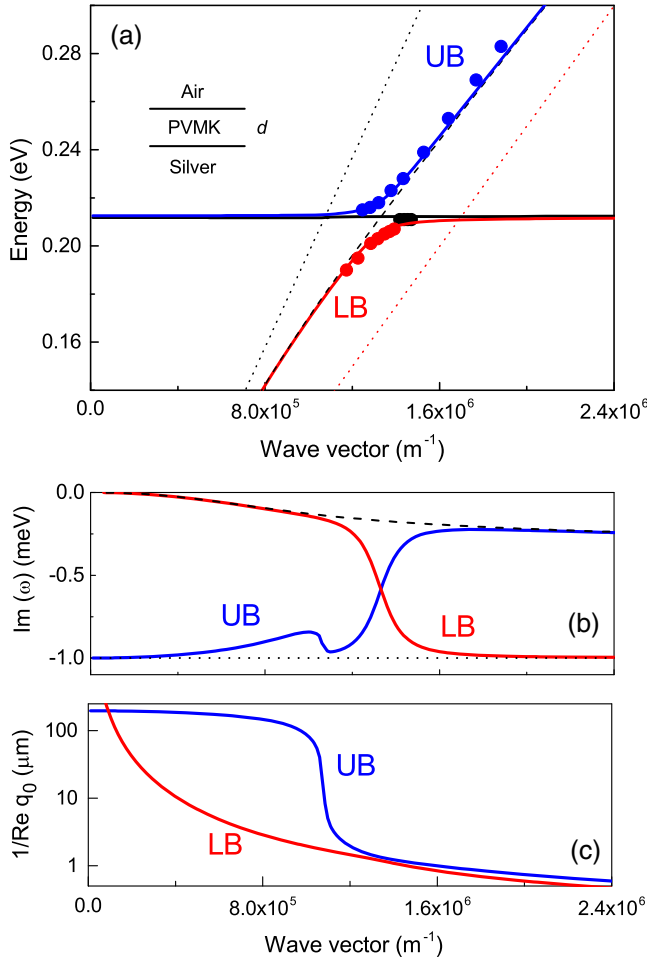


FIG. 3. Dispersion relation of a PVMK/silver hybrid structure in the strong coupling regime ( $d = 965$  nm). UB, upper branch (blue); LB, lower branch (red); middle branch (black). (a) Circles: Experimental ATR minima. Full curves: Dispersion ( $\text{Re } \omega$ ) calculated with the molecular resonance [ $\epsilon_1(\omega) = \epsilon_m$ ]. Dashed curve: Dispersion ( $\text{Re } \omega$ ) calculated without the molecular resonance [ $\epsilon_1(\omega) = \epsilon_{bm}$ ]. Dotted curves: Light line in air (black) and PVMK (red). Inset: The configuration analyzed theoretically. (b) The calculated dissipation rate ( $\text{Im } \omega$ ). Full curve: With the molecular resonance. Dashed curve: Without the molecular resonance. Dotted line: The molecular dissipation rate. (c) Calculated penetration depths into air ( $1/\text{Re } q_0$ ). The dispersion relation is calculated from Eq. (4).

with  $\omega_0$ ,  $A$ , and  $\gamma$  being again the molecular parameters of Eq. (1) as well as  $\gamma_{\text{spp}}$  the dissipation rate of the uncoupled SPP. If  $A < (\gamma - \gamma_{\text{spp}})^2$ , the system is in the weak coupling regime and only the dissipation is modified. A finite energy splitting  $\Delta\omega = \omega_+ - \omega_-$  in Eq. (3) is obtained if  $A > (\gamma - \gamma_{\text{spp}})^2$ , observable in the experiment if the splitting is larger than the spectral width of the branches, i.e.,  $\Delta\omega > \gamma + \gamma_{\text{spp}}$ . This gives the condition for the strong coupling regime. While the splitting in resonance ( $k = 1.32 \times 10^6 \text{ m}^{-1}$ ) can be easily derived from the ATR minima to be 13 meV, the spectral width of the

branches needs to be carefully interpreted to conclude on the dissipation rate. First, as already stressed above, the branches are substantially broadened by the angular spread of the excitation beam. Second, since the spectra are collected at fixed  $\alpha$ , the features are further broadened compared to fixed wave vector scans. And third, resonance of the upper and lower branch is achieved at an angle of  $\alpha \approx 60^\circ$  and  $\alpha \approx 68^\circ$  for the upper and lower branch, respectively. Nevertheless, the spectral width of about 3 meV found on the bare experimental spectra is still clearly smaller than the splitting. A value of  $\Delta\omega = 17$  meV is derived when inserting the molecular parameters and the estimated dissipation rate of the SPP ( $\gamma_{\text{spp}} \approx 2$  meV) into Eq. (3), which is slightly larger than the experimental result because of the finite molecular layer thickness of our hybrid structure.

The above findings consistently evidence the strong coupling of SPPs and molecular vibrations. In order to understand the hybridization scenario in more detail, we consider the dispersion relation of SPPs in our hybrid structure. For two planar adjacent interfaces separated by the distance  $d$ , the dispersion relation is provided by the implicit expression [25]

$$(\beta_0 + \beta_1)(\beta_1 + \beta_2) + (\beta_0 - \beta_1)(\beta_1 - \beta_2)e^{-2q_1 d} = 0 \quad (4)$$

with  $\beta_j(\omega, k) = \epsilon_j(\omega)/q_j(\omega, k)$ ,  $j = 0, 1, 2$ , and  $\epsilon_0 = 1$  for air and  $\epsilon_1(\omega) = \epsilon_m(\omega)$  the dielectric function of the PVMK film with thickness  $d$ , as well as  $\epsilon_2(\omega) = \epsilon_p(\omega)$  the Drude function of silver. The out-of-plane wave vector component  $i q_j(\omega, k)$  results from  $q_j(\omega, k) = \sqrt{k^2 - (\omega/c)^2 \epsilon_j(\omega)}$ . The observed ATR minima of the hybrid sample are plotted in Fig. 3(a) together with the calculated dispersion relation. All branches observed in the experiment are reproduced by the numerical calculations. Far below the molecular resonance frequency, the dispersion of the lower branch is identical to that of the uncoupled SPP. When approaching the molecular resonance, the dispersion curve bends down and eventually ends up at  $\omega_0$  for an infinitely large in-plane wave vector. The upper branch evolves inside the light cone and merges with the uncoupled SPP dispersion for large in-plane wave vectors. For the present molecular layer thickness  $d$ , the minimum energy splitting between both branches is 13 meV. The hybridization scenario is also evident from the dissipation rate ( $\text{Im } \omega$ ) of the branches depicted in Fig. 3(b). For small wave vector values, the damping of the lower branch is identical to that of the uncoupled SPP. But when  $\text{Re } \omega$  draws near  $\omega_0$  the admixture of a vibrational component manifests in an increase of the dissipation rate, eventually coinciding with the molecular damping for  $k \rightarrow \infty$ .  $\text{Im } \omega$  of the upper branch, on the other hand, is identical to  $\gamma$  at  $k = 0$ . It approaches quickly the dissipation rate of the SPP when the wave vector is increased albeit a weak back bending

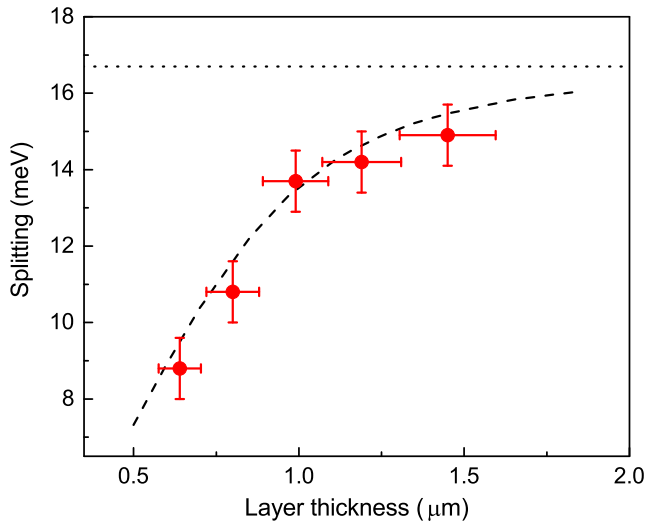


FIG. 4. Dependence of the energy splitting on the molecular film thickness. Red circles: Experimental results. Dashed line: Calculated from Eq. (4). Dotted line: Splitting of a hybrid structure with an infinitely thick PVMK layer calculated from Eq. (4) with  $\epsilon_1 = \epsilon_0 = \epsilon_m(\omega)$ .

appearing when  $\text{Re } \omega$  crosses the air-light line. The field penetration of the upper and lower branch into air remains always finite for  $k > 0$ , demonstrating the evanescent character of the hybrid species [Fig. 3(c)].

Figure 4 depicts the energy splitting as a function of the PVMK layer thickness  $d$ . Because the number of experimental data points is limited, we determined the splitting after interpolating the dispersion points of the upper and lower polariton branch. Again, the experimental data agree well with the numerical calculations. The energy splitting increases for thicker molecular films, but already at  $d > 1000$  nm saturation sets in and the splitting approaches the value of a hybrid structure with an infinitely thick molecular layer.

In conclusion, we have demonstrated the strong coupling of SPPs and molecular vibrations. This new electromagnetic and vibrational eigenstate is not only interesting from a fundamental point of view but also of direct practical relevance. It has been demonstrated that hybridization of microcavity photons and excitons in organic compounds offers the possibility to modify chemical reaction rates [26]. Recently, the same concept has been also applied to molecular vibrations [27,28]. By coupling to SPPs instead of microcavity photons, this approach can be transferred into a large-area and geometrically simple setting. The scenario is not restricted to the stretch vibration of the carbonyl group, and any infrared active vibrational transition with a strong optical dipole moment could be targeted. The modification of intramolecular relaxation rates is also of immediate interest for optoelectronic functionality. Moreover, vibrational energy, otherwise localized on a single molecule or side group, can now

be coherently transported along the surface for triggering electronic processes like exciton dissociation.

This work was supported by the Deutsche Forschungsgemeinschaft in the frame of SFB 951 (HIOS). The authors thank F. Intravia, K. Busch, B. Kobin, and S. Hecht for helpful discussions and K. Komander for AFM measurements. H.M. thanks the Graduate School Hybrid4energy of Humboldt-Universität zu Berlin and the Helmholtz-Zentrum Berlin für Materialien und Energie for funding.

- 
- [1] *Physics of Semiconductor Microcavities: From Fundamentals to Nanoscale Devices*, edited by B. Deveaud (Wiley-VCH, Weinheim, 2007).
  - [2] H. Deng, G. Weihs, D. Snoke, J. Bloch, and Y. Yamamoto, *Proc. Natl. Acad. Sci. U.S.A.* **100**, 15318 (2003).
  - [3] J. Kasprzak, M. Richard, S. Kundermann, A. Baas, P. Jeambrun, J.M.J. Keeling, F.M. Marchetti, M.H. Szymańska, R. André, J.L. Staehli, V. Savona, P.B. Littlewood, B. Deveaud, and Le Si Dang, *Nature (London)* **443**, 409 (2006).
  - [4] A. Amo, J. Lefrère, S. Pigeon, C. Adrados, C. Ciuti, I. Carusotto, R. Houdré, E. Giacobino, and A. Bramati, *Nat. Phys.* **5**, 805 (2009).
  - [5] W.L. Barnes, A. Dereux, and T.W. Ebbesen, *Nature (London)* **424**, 824 (2003).
  - [6] P. Törmä and W.L. Barnes, *Rep. Prog. Phys.* **78**, 013901 (2015).
  - [7] I. Pockrand, A. Brillante, and D. Mobius, *J. Chem. Phys.* **77**, 6289 (1982).
  - [8] J. Bellessa, C. Bonnand, J. C. Plenet, and J. Mugnier, *Phys. Rev. Lett.* **93**, 036404 (2004).
  - [9] C. Symonds, C. Bonnand, J.C. Plenet, A. Brehier, R. Parashkov, J. S. Lauret, E. Deleporte, and J. Bellessa, *New J. Phys.* **10**, 065017 (2008).
  - [10] P. Vasa, R. Pomraenke, S. Schwieger, Y.I. Mazur, V. Kunets, P. Srinivasan, E. Johnson, J.E. Kihm, D.S. Kim, E. Runge, G. Salamo, and C. Lienau, *Phys. Rev. Lett.* **101**, 116801 (2008).
  - [11] D. E. Gomez, K. C. Vernon, P. Mulvaney, and T. J. Davis, *Nano Lett.* **10**, 274 (2010).
  - [12] S. Abera Guebrou, C. Symonds, E. Homeyer, J. C. Plenet, Yu. N. Gartstein, V.M. Agranovich, and J. Bellessa, *Phys. Rev. Lett.* **108**, 066401 (2012).
  - [13] L. Shi, T. K. Hakala, H. T. Rekola, J.-P. Martikainen, R. J. Moerland, and P. Törmä, *Phys. Rev. Lett.* **112**, 153002 (2014).
  - [14] P. Vasa, W. Wang, R. Pomraenke, M. Lammers, M. Maiuri, C. Manzoni, G. Cerullo, and C. Lienau, *Nat. Photonics* **7**, 128 (2013).
  - [15] K. Kneipp, Y. Wang, H. Kneipp, L. T. Perelman, I. Itzkan, R. R. Dasari, and M. S. Feld, *Phys. Rev. Lett.* **78**, 1667 (1997).
  - [16] S. Nie and S. R. Emory, *Science* **275**, 1102 (1997).
  - [17] See, e.g., S. Schlücker, *Angew. Chem., Int. Ed.* **53**, 4756 (2014), and references therein.

- [18] S. Kalusniak, S. Sadofev, and F. Henneberger, *Phys. Rev. B* **90**, 125423 (2014).
- [19] A. Hartstein, J. R. Kirtley, and J. C. Tsang, *Phys. Rev. Lett.* **45**, 201 (1980).
- [20] A. Hatta, Y. Suzuki, and W. Sueteka, *Appl. Phys. A* **35**, 135 (1984).
- [21] For a recent study on this subject, see, for example, V. W. Brar, M. S. Jang, M. Sherrott, S. Kim, J. J. Lopez, L. B. Kim, M. Choi, and H. Atwater, *Nano Lett.* **14**, 3876 (2014).
- [22] H. H. Li, *J. Phys. Chem. Ref. Data* **9**, 161 (1980).
- [23] J. H. Weaver, C. Krafka, D. W. Lynch, and E. E. Koch, *Optical Properties of Metals, Part II, Physics Data No. 18-2* (Fachinformationszentrum Energie, Physik, Mathematik, Karlsruhe, 1981).
- [24] The angular spread of the excitation beam is taken into account in the TRMA calculations by averaging over 80 spectra calculated for different angles of incidence. Each spectrum is weighted by a Gaussian function centered at the experimental angle of incidence  $\alpha$  and with a standard deviation of  $1.75^\circ$ .
- [25] S. A. Maier, *Plasmonics: Fundamentals and Applications* (Springer, New York, 2007).
- [26] J. A. Hutchison, T. Schwartz, C. Genet, E. Devaux, and T. W. Ebbesen, *Angew. Chem., Int. Ed.* **51**, 1592 (2012).
- [27] A. Shalabney, J. George, J. Hutchison, G. Puppillo, C. Genet, and T. W. Ebbesen, *Nat. Commun.* **6**, 5981 (2015).
- [28] J. P. Long and B. S. Simpkins, *ACS Photonics* **2**, 130 (2015).